Lindsay J. Morrison, Julia Chatmot-Rooke, Vicki H. Wysocki

Diketopiperazine and oxazolone structures: an investigation of the influence of the third residue on b_2 structure in QAXIG and NAXIG analogues

Graphical Abstract

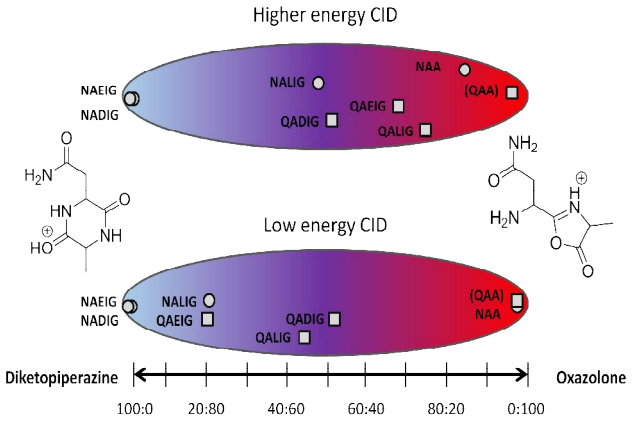

Abstract

Variables impacting the formation of b_2 ions along the "diketopiperazine" pathway are explored using IRMPD action spectroscopy and gas-phase hydrogen-deuterium exchange for a series of QAXIG and NAXIG pentapeptide analogues. The b_2 ion is a unique fragment in peptide fragmentation because it can be one of two main isobaric structures, the diketopiperazine or the oxazolone. The formation of these has been thought to be largely governed by the identity of the first two residues at the N-terminus of the peptide. We show here that a basic residue is not required for the formation of the diketopiperazine structure, as the amide side chain of a glutamine or asparagine residue is implicated in the formation of this structure. Furthermore, the length of the peptide and identity of the third residue of the peptide is shown for the first time to influence the diketopiperazine:oxazolone ratio.

Introduction

The details of gas phase peptide fragmentation pose an intriguing challenge both fundamentally and practically. The chemistry inherent to mass spectrometry fragmentation is incompletely understood and solution and gas phase molecules can exhibit very different behaviors.[1-2] Peptides are an ideal medium with which gas phase chemistries can be explored. Solid phase FMOC and BOC-based chemistries permit peptides to be synthesized in an almost unlimited number of motifs and functionalities, allowing fragmentation chemists to design custom systems and isolate desired phenomena. Practically, understanding peptide fragmentation is of high interest in the field of proteomics, wherein mass spectrometry and tandem mass spectrometry have become invaluable tools. In a proteomics experiment, tandem mass spectra are collected so that peptide sequences can be assigned from the fragmentation pattern of the precursor, inferring protein identifications. Because a single proteomics experiment typically generates thousands of spectra, interpretation and sequence assignment has been relegated to the domain of sequencing algorithm interpretation programs such as MASCOT and SEQUEST.[3-5] These algorithms are based on the understanding of peptide fragmentation, but tend to use simplistic fragmentation models to assign spectra.

As the ratio of assigned sequences to generated spectra remains modest at best, a number of strategies are being developed to improve both spectral quality, algorithm efficiency, and database approaches. While the more popular algorithms often trade processing speed for model complexity, a new trend is emerging to develop programs that incorporate non-standard fragmentation pathways and ion intensity into the algorithm.[6-8] Fundamental experiments continue to increase the understanding of the enhancement and suppression of fragmentation at particular residues and this understanding adds confidence to sequence assignments. Omission of

ion intensity in these routines, as is often done, forfeits the increased confidence in the sequence assignment. Further development of algorithms along these lines will demand a more thorough understanding of fragmentation behavior, as the chemistry that governs the variations in ion intensity is still only partially understood.

The standard fragmentation pathway of protonated peptides by CID occurs at the backbone amide bond, generating a series of "b" and "y" type ions, wherein the C-terminal fragment or y ion is a truncated peptide and the N-terminal portion forms a cyclic structure. Yalcin and co-workers first proposed a 5-membered oxazolone ring as the dominant b ion structure using kinetic energy release data; this structure was later confirmed using a combination of computational modeling and action IRMPD spectroscopy by Polfer and co-workers.[9-13] Later studies using action IRMPD and hydrogen-deuterium exchange (HDX) on YGGFL, YAGFL, and oligoglycine provided evidence for low abundance macrocyclic structures in b ion populations.[14-16] These structures are able to rearrange into a number of oxazolone structures, effectively scrambling the sequence of the peptide. For this reason, they received much attention over subsequent years.[16-24]

The smallest of these cyclic peptide structures, the b_2 diketopiperazine, has been particularly well-studied, not because of its role in sequence scrambling, but rather because it requires an unusual trans-cis isomerization step prior to its formation.[25-26] This isomerization step adds an interesting chemical feature unique to the b_2 ion: although the diketopiperazine is typically thermodynamically more stable, trans-cis isomerization adds a kinetic barrier to the formation of diketopiperazine.[27-28] The typical result is an interplay in which the thermodynamic (diketopiperazine) and kinetic product (oxazolone) are variably formed, although the kinetic pathway is typically followed in CID experiments. However, a number of studies have shown

that residue identity plays an influential role in favoring or disfavoring these pathways. Wysocki and coworkers have shown evidence indicating that the diketopiperazine structure is present in low abundance for the AP, IP, and VP systems, concluding that the more cis character of the proline amide bond makes diketopiperazine formation more favorable.[29-32] A vast body of work has gone into histidine containing b_2 systems, and it has been shown that HA, AH, HG, and GH all form mixtures of diketopiperazine and oxazolone structures while HP forms exclusively diketopiperazine.[26,33-34] The Polfer lab has recently demonstrated that an arginine residue in the first or second position also makes diketopiperazine formation competitive in b_2-H_20 ions.[35] Although b_2 ions that contain only aliphatic and aromatic residues have been shown to feature exclusively oxazolone structures,[36-38] a basic residue in residue positions 1 or 2 has been shown to allow trans-cis isomerization and diketopiperazine formation.[33,35]

In this paper we explore the effects of N-terminal glutamine or asparagine and a variable third residue in pentapeptide systems on diketopiperazine and oxazolone formation using a combination of HDX and action IRMPD spectroscopy. Being non-basic, glutamine and asparagine are not capable of sequestering the mobile proton as well as a basic residue, but both possess an amide side chain with varying lengths that permit a variety of proton bridging chemistries. The impact of the remaining peptide chain on the formation of b_2 ions has largely been disregarded in studies of b_2 ions. In this study, systems of sequence QAXIG and NAXIG, with the third residue being either an acidic residue (glutamic or aspartic acid) or an aliphatic residue (leucine) are examined using action IRMPD spectroscopy and gas-phase hydrogen/deuterium exchange. Acidic residues were selected in order to study the effect of a flexible and reactive side chain at the third position while simultaneously avoiding conflicting data arising from usage of a basic residue such as histidine or lysine. A pentapeptide scaffold

was additionally chosen in order to more accurately examine the behavior of longer peptides typically observed in proteomics experiments.

Material and Methods

Peptide synthesis

FMOC protected amino acids were obtained from Novabiochem (San Diego, CA) and peptides were synthesized in-house using standard FMOC solid phase synthesis techniques.[39] The C-terminal, resin-linked residue was used without purification and treated with dimethylformamide (DMF) to swell the polymer bead. The FMOC protecting group was removed from the growing peptide by washing with 70:30 DMF:piperidine solvent. Coupling was performed in a stepwise manner using -benzotriazole-N,N,N',N'-tetramethyl-uronium-hexafluoro-phosphate (HBtU) and *N*,*N*-diisopropylethylamine (DIEA) to promote formation of the amide bond. Peptides were cleaved from the resin by incubation in 95% trifluoracetic acid and were extracted twice with diethyl ether. Purified peptides were then diluted into 50:50:0.1% Acetonitrile:H_20:formic acid electrospray solvent before introduction into the mass spectrometer.

Mass spectrometry

Deuterated ammonia was used for all gas-phase hydrogen/deuterium exchange (HDX) studies and was obtained from Sigma-Aldrich (St. Louis, MO). Fragmentation and hydrogen/deuterium exchange studies were performed on a Thermo Scientific Velos Pro dual linear ion trap. Following introduction to the gas phase by an electrospray source, precursor ions were monoisotopically mass selected in high pressure region of the trap and fragmented by HCD to generate the b_2 ions. Gas-phase hydrogen/deuterium exchange (HDX) was performed by saturating the trap with deuterated ammonia and subsequently flushing with helium to generate a

low ambient pressure of deuterated ammonia that remained relatively constant for several minutes. The exchange of leucine-enkephalin for 10ms was used to monitor this pressure and incubation of the analyte b_2 ions was performed in triplicate in all experiments for 2 minute intervals using a deuterated ammonia pressure that resulted in 5% exchange of leucine-enkephalin.

Action IRMPD spectroscopy was performed using a trapping mass spectrometer coupled to a free electron laser at the CLIO facility in Orsay, France. Ions were introduced to the gas phase using electrospray ionization and protonated precursor molecules transmitted to the ion trap for CID and IRMPD. A Bruker Daltonics Esquire 3000^+ ion trap was used coupled to a free electron laser was used for QAXIG experiments and a Bruker Daltonics 7T FT-ICR was used for NAXIG peptides. QAXIG precursor ions were mass selected and fragmented within the ion trap to generate b_2 ions and NAXIG b_2 ions were generated by quadrupole CID prior to entering the ICR cell. Once generated, b_2 ions were subjected to 110 ms macropulses of irradiation from the free electron laser, each of which was comprised of 12, nanosecond timescale micropulses. Typical laser energies were 450-600 mW. Following macropulse irradiation, fragment and precursor ions were detected using was ion trap or FT-ICR analyzers. Single spectra were acquired for NAXIG peptides and duplicate spectra for QAA and QAXIG peptides. Spectra were generated by plotting the fragmentation efficiency of the b_2 ion against irradiation frequency.

Computations

Optimizations and frequency calculation were performed using the Gaussian 09 software package with a B3LYP/6-311++G** basis set. Preliminary conformations of oxazolone and diketopiperazine structures were obtained using a conformation search function within the

Macromodel software package.[40] Collections of conformations were generated for both the diketopiperazine and oxazolone classes of molecules, considering all amine nitrogens and amide oxygens as potential protonation sites. Redundant conformers were eliminated at the B3LYP/6-31G level if they shared identical bridging with another conformer and were greater than 12 kcal/mol higher in energy than the lowest energy conformer. Final frequency spectra were scaled by 0.978 and the full-width at half-maximum peak width adjusted to 10 cm^{-1} to best correlate with experimental spectra.

Results

Comparison of NAA and NAXIG systems

Systems featuring an N-terminal asparagine or glutamine have been shown previously by Stein and coworkers to fragment via abundant water and ammonia loss pathways.[41-42] The fragmentation behavior of the NAEIG b_2 ion by CID is consistent with their findings (Figure S1(a)). The b_2 ion shows dominant fragment ion peaks at m/z 169 ($-NH_3$), 168 ($-H_20$), 158 (-CO), 141 ($-CO-NH_3$), and 140 ($-CO-H_20$) representative of two major fragmentation pathways: water/ammonia loss, CO loss to form the a_2 ion, and a combination of the two.

Action IRMPD spectroscopy was obtained for the b_2 ion from peptide analogues of sequence NAA and NAXIG, wherein X was glutamic acid, aspartic acid, or leucine. The NAXIG b_2 ion action IRMPD spectra are shown in Figure 5 (a) – (c). The IRMPD spectrum for the b_2 ion of NAA is shown in Figure 5(d) and is in excellent agreement with the calculated IR spectrum of the ring protonated oxazolone structure shown in Figure 5(f). From inspection of the four experimental IRMPD spectra in Figure 5 (a)-(d), clear differences in the b_2 absorption behavior are evident in the 1500-2000 cm^{-1} range. The b_2 ions from both NAEIG and NADIG exhibit

dominant absorption bands at 1420, 1600, and 1750 cm^{-1} while the b_2 population from NAA features dominant absorption bands at 1610 and 1690, as well as a weak band at 1900, that corresponds to a ring carbonyl stretching mode and is diagnostic of an oxazolone structure. Laser power in this range is extremely weak and this band typically appears lower in intensity than predicted by DFT calculations. The b_2 population from NALIG exhibits absorption modes consistent with both the NAA and NA(D/E)IG type spectra, suggesting that it is composed of a mixture of structures.

The diagnostic absorption bands at 1420, 1600, and 1750 cm^{-1} exhibited by the b_2 ions from NADIG and NAEIG are in relatively good agreement with the amide stretching modes of the carbonyl protonated diketopiperazine structure shown in Figure 5(e), although the calculated band at 1750 cm^{-1} is blue shifted by 10 cm^{-1} relative to the experimental band. The lowest energy diketopiperazine structure for this system has the charging proton participating in a hydrogen bond between the asparagine backbone carbonyl oxygen and the side chain carbonyl oxygen. The DFT calculated spectrum for this structure is an exceptionally poor match to the experimental and was therefore discarded. It is shown in Supplementary Information Figure S2 in comparison to the experimental NAXIG spectra. The second lowest diketopiperazine structure has the charging proton located on the alanine carbonyl oxygen and is 8 kcal/mol higher in energy than the lowest energy diketopiperazine structure. This diketopiperazine structure is, however, 5 kcal/mol lower in energy than the lowest energy oxazolone structure. The amide stretching mode at 1780 cm^{-1} predicted by DFT calculations is seen to be in excellent agreement with the experimental NA(D/E)IG b_2 spectra. Although the placement of the predicted bands at 1600 and 1690 cm^{-1} are in agreement with the experimental NADIG and NAEIG b_2 spectra, the relative intensity of these bands are do not agree well with the experimental spectrum. However,

poor agreement of theoretical and experimental band intensities has been observed frequently in action IRMPD experiments.[35,43-45] For example, the predicted NH_2 scissoring mode at 1600 cm^{-1} is anticipated by DFT to be very weak, but appears as one of the strongest bands in the experimental spectrum. We have observed highly intense NH_2 scissoring modes in our studies of other peptide systems.[33,46] The b_2 ion populations from NAEIG and NADIG thus appear to be exclusively diketopiperazine and are the first evidence showing a non-basic residue in one of the first two residue positions (asparagine) contributing to dominant diketopiperazine formation.

The dominant absorption bands for the b_2 ions of NAEIG and NADIG are in clear contrast with the diagnostic oxazolone stretching modes at 1620 and 1690 cm^{-1} observed in the NAA b_2 ion spectrum. The NALIG spectrum appears as a composite of the NA(E/D)IG and NAA b_2 experimental spectra, with bands at 1420, 1600, 1690, and 1750 cm^{-1}, suggesting a roughly equal mixture of diketopiperazine and oxazolone structures. These results unequivocally demonstrate that the length and structural composition of the precursor peptide impacts the type of b_2 ion formed. However, because the NAA precursor varies both in peptide length and side chain identity of the third residue, it is not possible to attribute the presence of diketopiperazine b_2 in the NALIG system to either variable alone. The trend for the acidic amino acid systems, however, is very clear: the acidic residue in the third position causes the diketopiperazine structure to be exclusively favored.

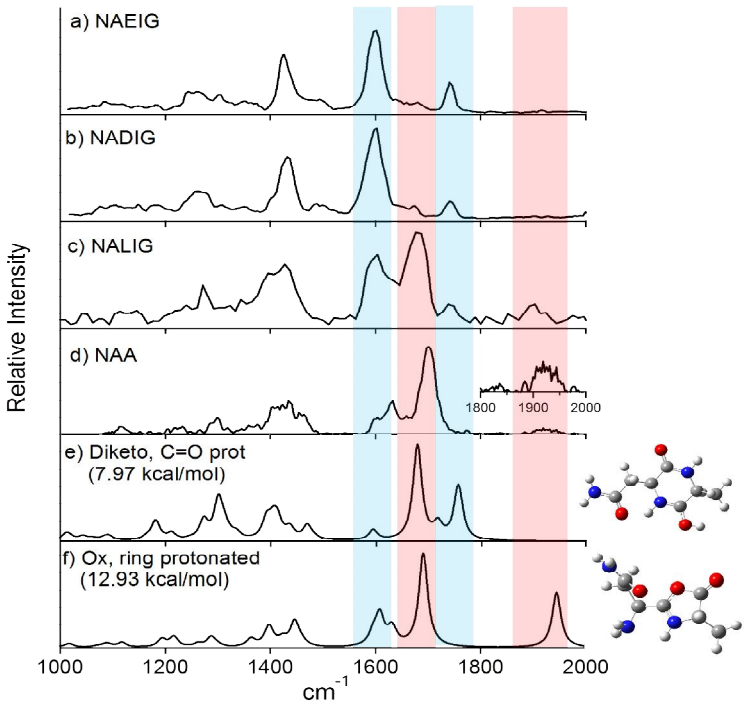

Figure 1: Action IRMPD spectra from the b_2 ion of a) NAEIG, b) NADIG, c) NALIG, and d) NAA. The theoretical IR spectra for the second lowest energy diketopiperazine and lowest energy oxazolone structures are shown in (e) and (f) respectively.

Glutamine-containing systems: QAXIG

Figure 2 shows a comparison of the action IRMPD spectra of the b_2 ions from the (a) QALIG, (b) QADIG, and (c) QAEIG peptide analogues. The range from 1000 to 2000 cm^{-1} can be seen to be complex with intense bands at 1610, 1670, 1780, and 1900 cm^{-1}. Dominant bands a t 1610 and 1788 cm^{-1} are present in all spectra and suggest all three analogues share, in part, a common b_2 structure. However, the bands at 1670 and 1900 cm^{-1} are prominent only in the QADIG b_2 spectrum and suggest the presence of a second structure for this analogue. As before, the appearance of a band at 1900 cm^{-1} suggests that this second structure is an oxazolone. A small peak at 1670 cm^{-1} is present in the QALIG spectrum suggests small amounts of oxazolone

are present in this system. The absence of the 1900cm^{-1} peak in this spectrum can be attributed to a combination of low FEL laser power in this range and the low abundance of the oxazolone population.

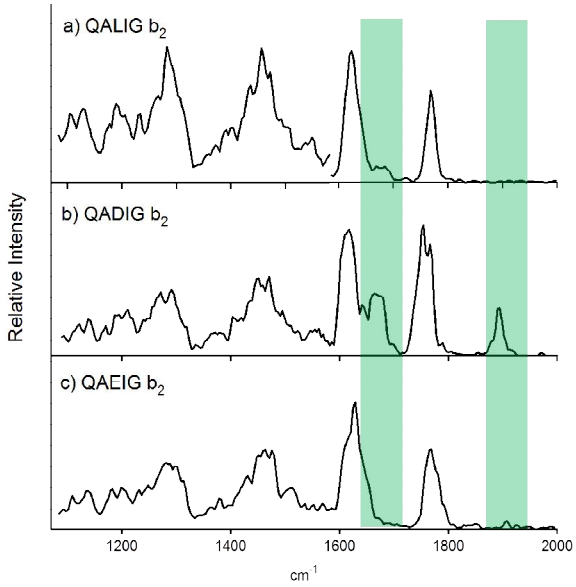

Figure 2: Action IRMPD spectra of the b_2 ions from (a) QALIG, (b) QADIG, and (c) QAEIG. Bands at 1670 and 1900 cm^{-1} suggest and oxazolone structure is present in the QALIG and QADIG b_2 populations.

Computational modeling of the QA oxazolone and diketopiperazine b_2 structures was performed in order to better interpret the spectra shown in Figure 2. Figure 3 shows a comparison between the experimental QADIG action IRMPD spectrum and theoretical oxazolone and diketopiperazine structures. In the lowest energy diketopiperazine structure, the charging proton is bound between the side chain amide oxygen and the proximal diketopiperazine carbonyl oxygen. Due to the flexibility of the glutamine side chain, several conformations are accessible to this structure. The theoretical IR spectra for the two most stable

conformations are shown in Figure 3(a) and (b) and make it apparent that movement of this side chain has a profound impact on the absorption spectrum of the molecule. For this reason, it is not possible to assign the experimental spectrum to a single conformer of this diketopiperazine structure. However, Figure 3(c) shows an empirical overlay composed of 70% diketo B and 30% diketo A that shows relatively good agreement with the bands at 1610 and 1780 cm^{-1}. The experimental spectrum features several bands between 1400 and 1600 cm^{-1} that are more coalesced than theory predicts, but small red or blue shifts due to coupling could account for these deviations. Comparison of the experimental spectrum with the theoretical oxazolone spectrum shows good agreement of the bands at 1670 and 1900 cm^{-1} with the oxazolone amide and ring carbonyl stretching modes and confirms the presence of the oxazolone structure in the QADIG b_2 population. Thus, the QADIG b_2 ion population is a mixture of carbonyl protonated diketopiperazine and N-terminally protonated oxazolone structures.

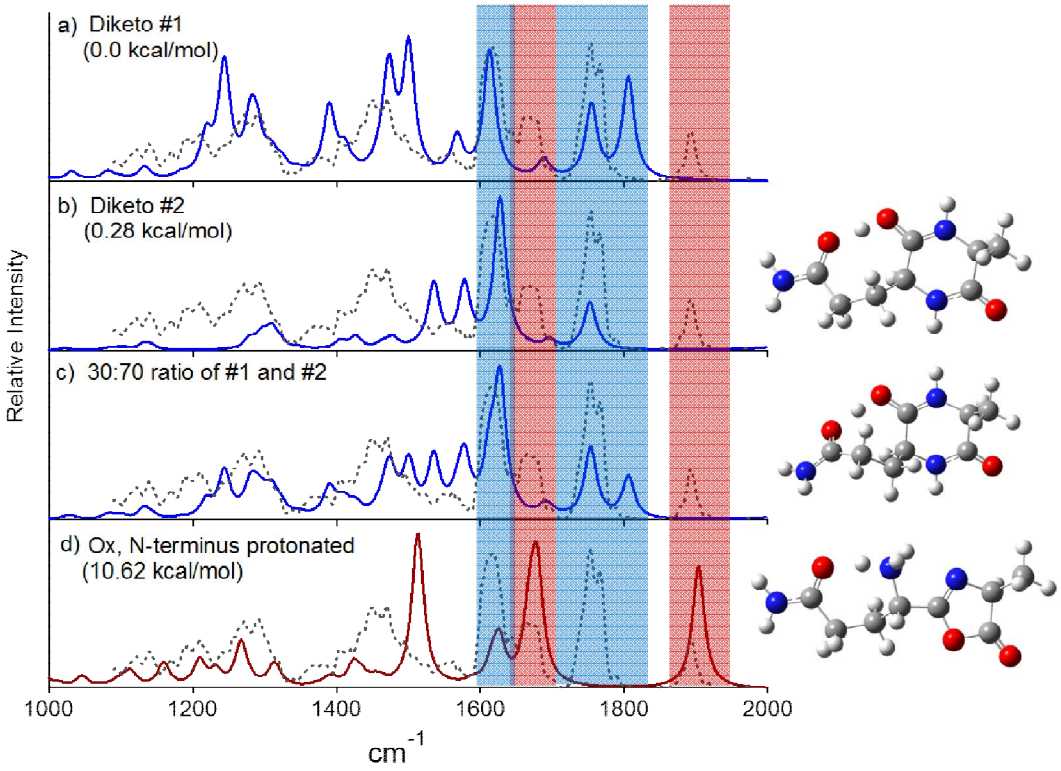

Figure 3: The two lowest energy diketopiperazine conformations are shown in (a) and (b), an empirical combination of (a) and (b) is shown in (c), and the N-terminally protonated oxazolone is shown in (d). The experimental action IRMPD spectrum of the b_2 of QADIG is overlaid in hashed lines over all four theoretical spectra.

Extrapolation of the comparison between the experimental QADIG b_2 and theoretical oxazolone and diketopiperazine in Figure 3 to the experimental QAXIG spectra in Figure 2 suggests that the dominant QA b_2 structure is the diketopiperazine. Although it is difficult to quantify the relative population abundances by action IRMPD, it is evident that both QALIG and QADIG feature some amount of oxazolone, although it is of low abundance in the QALIG case. In order to enumerate the relative abundances of the two populations, hydrogen-deuterium exchange studies were performed and are described in detail below. It is clear, however, that despite the chemical similarity between glutamic and aspartic acid, the effect they have on the diketopiperazine: oxazolone ratio is profoundly different in the QAXIG systems. As both NADIG and NAEIG formed exclusively diketopiperazine in the NAXIG systems, the disparity between QADIG and NADIG suggests that the amide side chain plays a significant role in the oxazolone and diketopiperazine pathways. Moreover, these data suggest that the interactions in which the amide side chain can participate are highly dependent on the length of the side chain. The potential energy surfaces of the Q/NAXIG analogues are extremely complex and numerous pathways can lead to the oxazolone and diketopiperazine structures. Thus, additional systems need to be evaluated in order to better characterize this behavior.

Action IRMPD Comparisons between NAXIG and QAXIG systems

Despite the somewhat poor quality of the match of the experimental QA b_2 ion spectra with the DFT predicted diketopiperazine spectrum, comparison with NAXIG systems strongly supports the diketopiperazine assignment. The diagnostic diketopiperazine NH_2 scissoring and amide stretching modes that appear at 1600 and 1750 cm^{-1} in the NAXIG systems are blue shifted to 1610 and 1780 cm^{-1} in the QAXIG systems, but the relative ratios of these bands remains the same. The blue shift can be attributed to the diketopiperazine structures for the NA and QA systems having different protonation sites. In the QA diketopiperazine, the charging proton is located in a hydrogen bond between the glutamine backbone carbonyl oxygen and side chain carbonyl oxygen. In contrast, in the NA diketopiperazine, the charging proton is located on the alanine carbonyl oxygen. This is particularly interesting as this is not the lowest energy diketopiperazine structure. While this is unusual, it can readily be attributed to the relatively short asparagine side chain. Upon closure of the diketopiperazine ring, the mobile proton becomes one of the protons on what was formerly the N-terminus. Because proton transfer in the gas phase relies on chains of basic sites between which protons can "hop," the asparagine side chain must mediate transfer of the charging proton to the other side of the molecule due to the lack of intermediate basic sites. It is plausible that the length of the side chain may limit the extent to which it can perform this operation, causing the charging proton to be transported to the nearest basic site, the alanine carbonyl oxygen.

Hydrogen-deuterium exchange studies

Gas phase HDX was performed on the NAXIG and NAA peptide analogues following activation of the precursor at various collision energies in order to evaluate the influence of

energy on the formation of the diketopiperazine and oxazolone NA b_2 structures. For simplicity, this technique will be referred to as energy resolved HDX or ERHDX. The exchange distributions from these experiments are shown in Figure 4. All b_2 ions were incubated in deuterated ammonia for 500 ms, as this time features the strongest difference in oxazolone and diketopiperazine exchange behavior (see Supplementary Information, Figure S3). The b_2 generated via 4% activation of the NAA peptide (see Figure 4a), demonstrated to be dominantly oxazolone in action IRMPD experiments, exhibits an exchange pattern in which the dominant product incorporates three deuteriums into the molecule after 500 ms incubation with the deuterating reagent. At higher collision energies, the relative intensity of the D_0, D_1, and D_2 peaks rises to some extent, although the D_3 remains the dominant peak in the distribution. The rise of these peaks may be related to the appearance of a second population at higher activation energies. In stark contrast to the HDX distribution observed for the b_2 ion from NAA, the b_2 populations of NADIG and NAEIG (Figure 4 c and d) feature much slower hydrogen-deuterium exchange, with the dominant peak in the exchange distribution being the D_0 at all collision energies. The bimodal distribution observed for the b_2 ion from NALIG suggests that it is composed of a mixture of a less extensively and more extensively exchanging population. Interestingly, the more extensively exchanging population is observed to increase in relative abundance at higher collision energies.

In order to assign structures to the different distributions observed by HDX, the basicity of the functional groups of the diketopiperazine and oxazolone structures must be considered. The diketopiperazine structure features three amide functional groups, with 4 exchangeable protons on amide nitrogens and the charging proton located on amide oxygen. Because amide groups are non-basic, exchange with deuterated ammonia is predicted to be very slow. In

contrast, the oxazolone b_2 structure is composed of a side chain amide, a primary amine, and a ring imine functional group. The ring protonated oxazolone contains 2 exchangeable protons on the primary amine (N-terminus) and one on the ring imine, all of which would be expected to exchange rapidly with ammonia due to their similar gas phase basicity. Moreover, gas phase HDX-ECD experiments have shown that backbone amide groups exchange more slowly with ND_3 than the basic side chains and peptide termini.[47] Thus, the more extensively exchanging structure can be assigned to be the oxazolone and the less extensively exchanging structure the diketopiperazine. Although HDX does not directly show structure, in conjunction with action IRMPD measurements, in which NAA exclusively formed an oxazolone b_2, NAEIG and NADIG formed exclusively diketopiperazine b_2 ions, and NALIG formed a mixture, assignment of the less extensively and more extensively populations as diketopiperazine and oxazolone, respectively, is reasonable. In addition, our group has observed this trend in the HDX behavior of several oxazolone and diketopiperazine structures.[26,32,48]

From DFT modeling, the lowest energy diketopiperazine structure has the charging proton located in a hydrogen bond between the side chain amide oxygen and the alanine amide oxygen. However, the predicted IR spectrum for this structure is a particularly poor match with the experimental action IRMPD b_2 spectrum from NADIG and NAEIG. The second lowest energy structure, however, shows good agreement with the experimental action IRMPD spectra of the b_2 of NADIG and NAEIG. This structure features the charging proton localized on the asparagine backbone amide oxygen. This structure is 5 kcal/mol lower in energy than the most stable oxazolone structure (ring protonated). As action IRMPD spectroscopy of the NAXIG analogues shows no evidence for the different precursors producing oxazolone and diketopiperazine b_2 ions of differing protonation sites, the NA b_2 ions will have these same

oxazolone and diketopiperazine energies regardless of precursor. Thus, the differences in b_2 structure observed by HDX and action IRMPD for the NAA and NAXIG analogues can be attributed to variable ring closure and trans-cis isomerization barriers that may change depending on precursor structure. This suggests that the trans-cis isomerization and diketopiperazine ring closure events in the NAA system must have significantly higher energy transition states than does the oxazolone ring closure transition state. Thus, the lower energy diketopiperazine structure would not form at low energies and would only form to a small extent at higher energies, as is observed for the NAA b_2. As noted above, Armentrout and Paizs have shown that the barrier for diketopiperazine ring closure in the GG and GGG systems is significantly higher than the oxazolone ring closure barrier, which is consistent with this behavior.

The b_2 oxazolone structure does not form for the NADIG and NAEIG analogues, suggesting that trans-cis isomerization and diketopiperazine ring closure barriers are much lower in energy than the oxazolone ring closure barrier for these analogues. The NALIG system is perhaps the most interesting of the NAXIG analogues, as variable amounts of oxazolone and diketopiperazine form depending on the activation energy used to generate the b_2. At low energies, the diketopiperazine is favored, whereas the higher energies favor the oxazolone structure. This trend is somewhat counter-intuitive because computational studies performed by Armentrout and Paizs, in which it was shown that the diketopiperazine has a significantly higher ring closure barrier than does the oxazolone structure, would suggest that the thermodynamic product would form more abundantly at higher energies.[28,49] One explanation for this behavior is that the oxazolone has a higher ring closure barrier but also a higher density of states. Thus, at low energies, the lower energy pathway is favored, whereas at higher energies the oxazolone ring closure transition state is more populated, causing the oxazolone to form with higher abundance.

Figure 6 shows a diagram in which the ring closure barriers are predicted based on these experiments. The density of states explanation for this behavior suggests that degrees of freedom in the bridging conformations of the oxazolone and diketopiperazine ring closure transition states may be a critical factor in discriminating which b_2 structure forms in N-terminal asparagine systems.

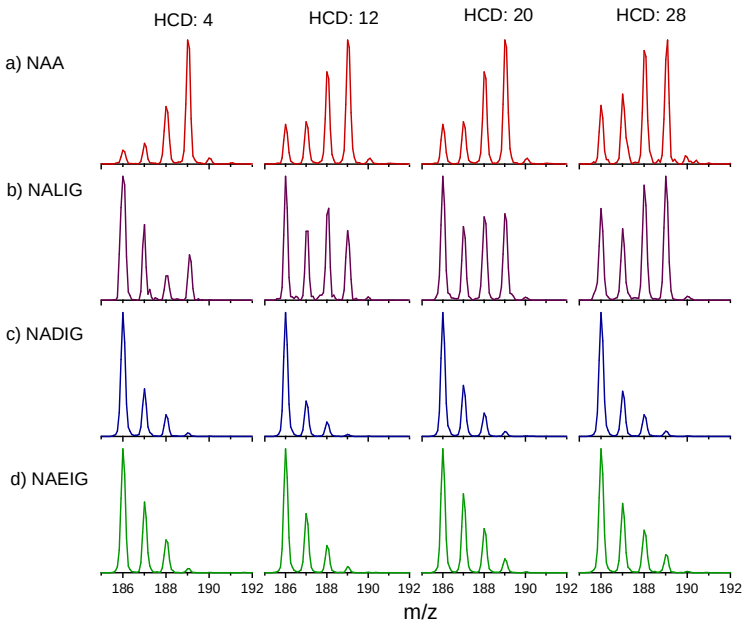

Figure 4: HDX of the b_2 population of NAA (a), NALIG (b), NADIG (c), and NAEIG (d) analogues following generation by HCD at various collision energies.

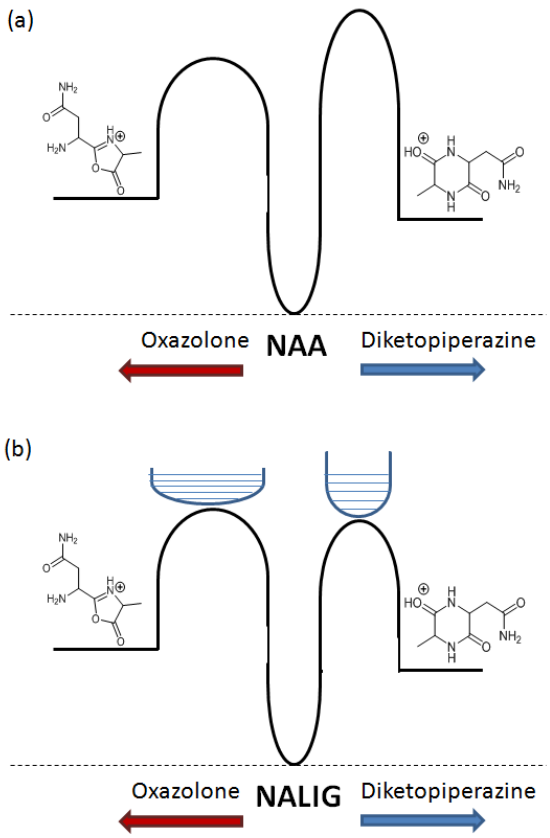

Figure 5: Diagram showing estimated ring closure barriers for the formation of oxazolone and diketopiperazine b_2 ion structures for (a) NAA and (b) NALIG based on ERHDX data and computational modeling of NA b_2 oxazolone and diketopiperazine structures.

ERHDX was performed on the QAA, QALIG, QADIG, and QAEIG analogues and results are shown in Figure 6. Because of the low abundance of the b_2 ion from the QAA system, acquisition of an action IRMPD spectrum of this b_2 ion was not feasible, however, it was possible to obtain HDX. As with the NAA system, the HDX of the b_2 from QAA features rapid exchange in which three exchanges dominate after 500 ms, suggesting QAA forms an oxazolone b_2 structure. Computational modeling of the QA oxazolone and QA diketopiperazine indicates that the lowest energy oxazolone (N-terminally protonated) is 10.6 kcal/mol higher in energy than the lowest energy diketopiperazine. However, the exchange distribution of the QAA b_2 does

not reflect a change in b_2 population over energy, as the distribution appears relatively constant over the energy range studied. The constancy of this pattern over a range of energies suggests that the barrier for diketopiperazine ring closure is significantly higher than the oxazolone ring closure barrier in this system. The pattern using 28% HCD energy appears somewhat different from the other energy points, with the distribution centering on the D_1 peak; however, the relative abundance of the b_2 at this energy is less than 1% and the low signal to noise ratio of the peak may contribute to the unusual oxazolone distribution.

Based on ERHDX, the b_2 population from all of the QAXIG analogues is a clear mixture of two structures, presumably oxazolone and diketopiperazine, across all energies. The behavior of these systems at low energies agrees well with action IRMPD data, where QALIG and QAEIG form a dominant diketopiperazine b_2 and QADIG generates a more even mixture of oxazolone and diketopiperazine. However, ERHDX suggests that the b_2 population from QALIG and QAEIG both shift to a dominant oxazolone population at high collision energies. This behavior is similar to that observed in the NALIG system, and may again be related to the density of states in the oxazolone and diketopiperazine ring closure transition states. In contrast, however, the b_2 population from QADIG can be seen to shift very little by ERHDX, although small increases in diketopiperazine are observed with increasing collision energy. A comprehensive computational study is needed to elucidate the structural details of the precursor peptides, the heights of these barriers, and the transition state structures, but such a study is computationally expensive and beyond the scope of this paper. Nonetheless, ERHDX of the (Q/N)AXIG and (Q/N)AA analogues demonstrates that peptides with an N-terminal ***amide*** residue feature b_2 oxazolone and diketopiperazine ring closure barriers that are exceptionally close in energy. Moreover, the relative abundance of the diketopiperazine and oxazolone b_2

structures can be altered by manipulation of the chemistry of the first and third residue and the length of the peptide.

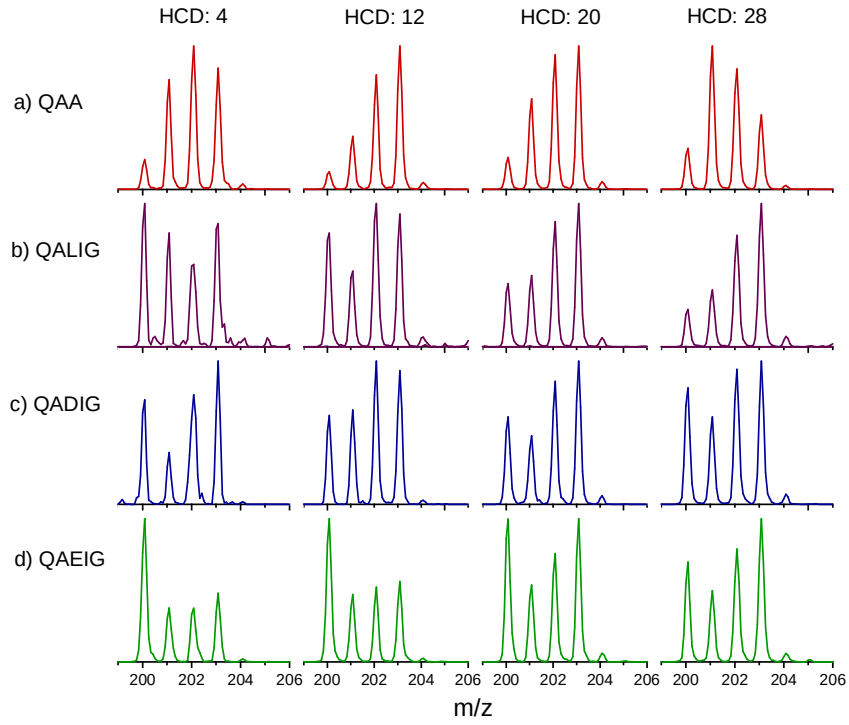

Figure 6: HDX of the b_2 population of QAA, QALIG, QADIG, and QAEIG analogues following generation by HCD at various collision energies.

Figure 7 shows the relative diketopiperazine abundance following activation over a range of energies for the NAXIG, QAXIG, QAA, and NAA systems. Population abundances were calculated using the ratio of the D_0 and D_3 peaks in the HDX distribution of each system. Because the presumed oxazolone population is centered at D_3 and the presumed diketopiperazine at D_0, this method gives a semi-quantitative approximation of the population abundance of each structure. Inspection of the plot shows that the diketopiperazine structure is ubiquitous in the (Q/N)AXIG systems. Only in the tripeptides (NAA and QAA) is the b_2 oxazolone dominant

across the energy series. None of the pentapeptide analogues forms exclusively oxazolone, although the fragmentation pathways followed by the NALIG, QALIG, and QAEIG analogues are observed to dramatically change as a function of collision energy. Only in the QADIG system does a mixture of oxazolone and diketopiperazine form and remain constant across the energy series. Although the formation of diketopiperazine and oxazolone type structures is competitive in this system, it is not obvious why. In the NAXIG series, the presence of an acidic third residue caused the diketopiperazine structure to be exclusively favored, but this trend is not present for the QAXIG systems, where increased collision energy increases the relative abundance of the oxazolone population for both QALIG and QAEIG. Density functional theory calculations confirm that the diketopiperazine structure is the thermodynamically favored product, but further investigation is necessary in order to probe the involvement of the amide and acid side chains in trans-cis isomerization and ring closure. Additional experimental studies are necessary to fully probe the effect of first position amide side chains and third position acid side chains.

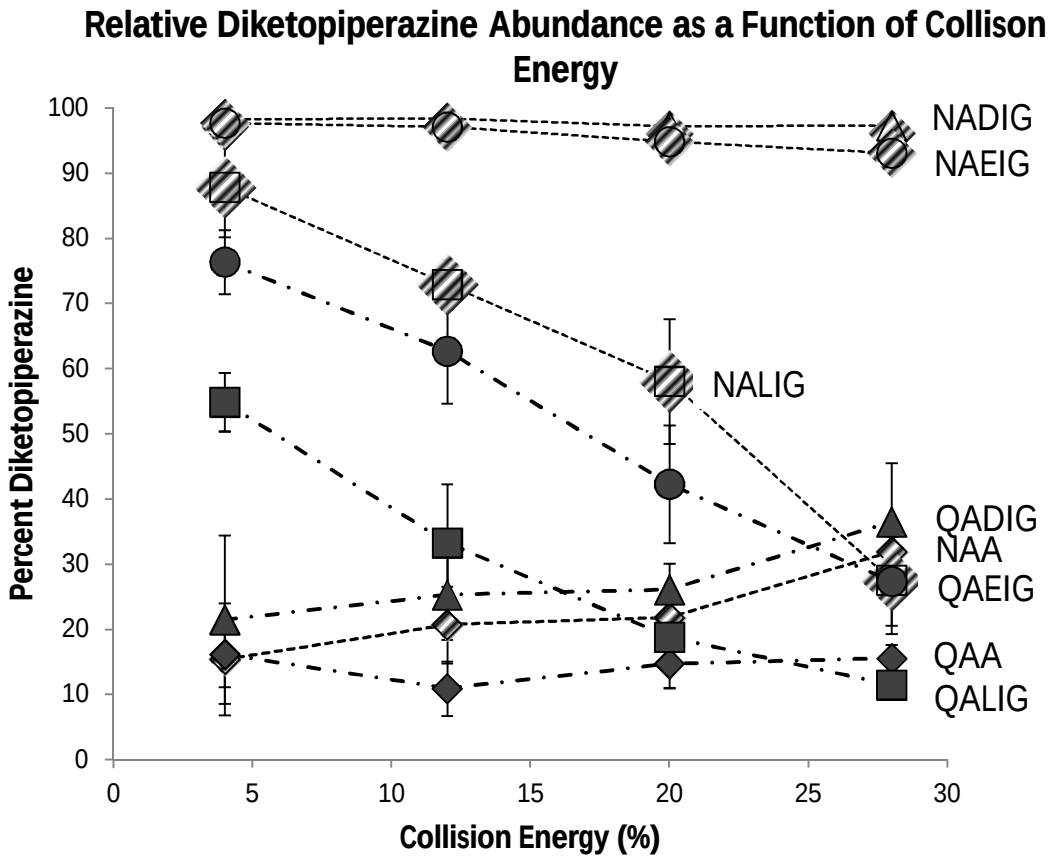

Figure 7: Relative b_2 diketopiperazine population abundance using 4%, 12%, 20%, and 28% HCD collision energy to generate b_2 from (Q/N)AXIG and (Q/N)AA analogues. Population abundances are roughly calculated based on the ratio of D_0 and D_3 in the ERHDX spectra.

Conclusions

Dominant diketopiperazine b_2 ion formation is demonstrated for the first time in amide-side chain containing systems. The non-basic side chain of glutamine and asparagine promotes diketopiperazine formation in pentapeptides of sequence (N/Q)AXIG. The identity of the third residue is additionally shown for the first time to be a factor in the preference for oxazolone vs. diketopiperazine formation. Leucine in the third position generates the greatest proportion of

oxazolone b_2 in both Q and N analogues, particularly at high collision energies, while aspartic acid in this position yields an almost exclusive b_2 diketopiperazine population in NADIG and a more dominant diketopiperazine population in QADIG. In contrast, the oxazolone predominantly forms in the QAA and NAA systems, suggesting that the length of the peptide may also be a factor in diketopiperazine vs. oxazolone formation. That oxazolone formation is more abundant in the leucine containing systems while diketopiperazine formation is more abundant in the aspartic acid containing systems may be related to either the hydrophobicity and steric bulk of the third position side chain or the bridging interactions in which both the acid and amide side chains can participate. A systematic study varying the length and chemical identity of the first and third residues and more extensive modeling of transition states is necessary in order to better understand the mechanistic details of this behavior.

References

(1) Sen, A.; Bouchet, A.; Lepere, V.; Le, B.-D. K.; Scuderi, D.; Piuzzi, F.; Zehnacker-Rentien, A. *J. Phys. Chem. A* **2012**, *116*, 8334.

(2) Eberlin, M. N.; Cooks, R. G. *J. Am. Chem. Soc.* **1993**, *115*, 9226.

(3) Perkins, D.; Pappin, D.; Creasy, D.; Cottrell, J. *Electrophoresis* **1999**, *20*, 3551.

(4) Eng, J. K.; McCormack, A. L.; Yates Iii, J. R. *Journal of the American Society for Mass Spectrometry* **1994**, *5*, 976.

(5) Martens, L.; Apweiler, R. *Methods Mol. Biol. (Totowa, NJ, U. S.)* **2009**, *564*, 245.

(6) Li, W.; Ji, L.; Goya, J.; Tan, G.; Wysocki, V. H. *Journal of Proteome Research* **2011**, *10*, 1593.

(7) Frank, A. M. *Journal of Proteome Research* **2009**, *8*, 2241.

(8) Tabb, D. L.; Fernando, C. G.; Chambers, M. C. *Journal of Proteome Research* **2007**, *6*, 654.

(9) Yalcin, T.; Csizmadia, I. G.; Peterson, M. R.; Harrison, A. G. *Journal of the American Society for Mass Spectrometry* **1996**, *7*, 233.

(10) Yalcin, T.; Khouw, C.; Csizmadia, I. G.; Peterson, M. R.; Harrison, A. G. *Journal of the American Society for Mass Spectrometry* **1995**, *6*, 1165.

(11) Polfer, N. C.; Oomens, J.; Suhai, S.; Paizs, B. *J. Am. Chem. Soc.* **2005**, *127*, 17154.

(12) Nold, M. J.; Wesdemiotis, C.; Yalcin, T.; Harrison, A. G. *Int. J. Mass Spectrom. Ion Processes* **1997**, *164*, 137.

(13) Yalcin, T.; Csizmadia, I. G.; Peterson, M. R.; Harrison, A. G. *J. Am. Soc. Mass Spectrom.* **1996**, *7*, 233.

(14) Chen, X.; Steill, J. D.; Oomens, J.; Polfer, N. C. *Journal of the American Society for Mass Spectrometry* **2010**, *21*, 1313.

(15) Chen, X.; Yu, L.; Steill, J. D.; Oomens, J.; Polfer, N. C. *J. Am. Chem. Soc.* **2009**, *131*, 18272.

(16) Gucinski, A. C.; Somogyi, A.; Chamot-Rooke, J.; Wysocki, V. H. *J. Am. Soc. Mass Spectrom.* **2010**, *21*, 1329.

(17) Molesworth, S.; Osburn, S.; Van Stipdonk, M. *Journal of the American Society of Mass Spectrometry* **2010**, 1028.

(18) Goloborodko, A. A.; Gorshkov, M. V.; Good, D. M.; Zubarev, R. A. *J Am Soc Mass Spectrom* **2011**, *22*, 1121.

(19) Atik, A. E.; Gorgulu, G.; Yalcin, T. *International Journal of Mass Spectrometry* **2012**, *316–318*, 84.

(20) Atik, A. E.; Yalcin, T. *J. Am. Soc. Mass Spectrom.* **2011**, *22*, 38.

(21) Saminathan, I. S.; Wang, X. S.; Guo, Y.; Krakovska, O.; Voisin, S.; Hopkinson, A. C.; Siu, K. W. M. *J. Am. Soc. Mass Spectrom.* **2010**, *21*, 2085.

(22) Bythell, B. J.; Knapp-Mohammady, M.; Paizs, B.; Harrison, A. G. *J. Am. Soc. Mass Spectrom.* **2010**, *21*, 1352.

(23) Molesworth, S.; Osburn, S.; Van, S. M. *J. Am. Soc. Mass Spectrom.* **2009**, *20*, 2174.

(24) Harrison, A. G. *J. Am. Soc. Mass Spectrom.* **2008**, *19*, 1776.

(25) Paizs, B.; Suhai, S. *Mass Spectrometry Reviews* **2005**, 508.

(26) Perkins, B. R.; Chamot-Rooke, J.; Yoon, S. H.; Gucinski, A. C.; Somogyi, A.; Wysocki, V. H. *Journal of the American Chemical Society* **2009**, 17528.

(27) Balta, B.; Aviyente, V.; Lifshitz, C. *J. Am. Soc. Mass Spectrom.* **2003**, *14*, 1192.

(28) Armentrout, P. B.; Heaton, A. L. *J. Am. Soc. Mass Spectrom.* **2012**, *23*, 632.

(29) Smith, L. L.; Herrmann, K. A.; Wysocki, V. H. *J. Am. Soc. Mass Spectrom.* **2006**, *17*, 20.

(30) Pal, D.; Chakrabarti, P. *Journal of Molecular Biology* **1999**, *294*, 271.

(31) Jorgensen, W. L.; Gao, J. *Journal of the American Chemical Society* **1988**, *110*, 4212.

(32) Gucinski, A. C.; Chamot-Rooke, J.; Steinmetz, V.; Somogyi, A.; Wysocki, V. H. *J. Phys. Chem. A* **2013**, *117*, 1291.

(33) Gucinski, A. C.; Chamot-Rooke, J.; Nicol, E.; Somogyi, A.; Wysocki, V. H. *J. Phys. Chem. A* **2012**, *116*, 4296.

(34) Farrugia, J. M.; Taverner, T.; O'Hair, R. A. J. *Int. J. Mass Spectrom.* **2001**, *209*, 99.

(35) Zou, S.; Oomens, J.; Polfer, N. C. *Int. J. Mass Spectrom.* **2012**, *316-318*, 12.

(36) Oomens, J.; Young, S.; Molesworth, S.; van Stipdonk, M. *Journal of the American Society for Mass Spectrometry* **2009**, *20*, 334.

(37) Bythell, B.; Somogyi, Á.; Paizs, B. *Journal of the American Society for Mass Spectrometry* **2009**, *20*, 618.

(38) Yoon, S. H.; Chamot-Rooke, J.; Perkins, B. R.; Hilderbrand, A. E.; Poutsma, J. C.; Wysocki, V. H. *Journal of the American Chemical Society* **2008**, *130*, 17644.

(39) *Solid-Phase Peptide Synthesis: A Practical Approach*; Atherton, E.; Sheppard, R. C., Eds.; Oxford University Press: Oxford, 1989.

(40) Schrödinger, L.; 9.9 ed. New York, NY, 2011.

(41) Godugu, B.; Neta, P.; Simon-Manso, Y.; Stein, S. E. *J. Am. Soc. Mass Spectrom.* **2010**, *21*, 1169.

(42) Neta, P.; Pu, Q.-L.; Kilpatrick, L.; Yang, X.; Stein, S. E. *J. Am. Soc. Mass Spectrom.* **2007**, *18*, 27.

(43) Chiavarino, B.; Crestoni, M. E.; Fornarini, S.; Scuderi, D.; Salpin, J.-Y. *J. Am. Chem. Soc.* **2013**, *135*, 1445.

(44) Wang, D.; Gulyuz, K.; Stedwell, C. N.; Yu, L.; Polfer, N. C. *Int. J. Mass Spectrom.* **2012**, *330-332*, 144.

(45) Martens, J. K.; Compagnon, I.; Nicol, E.; McMahon, T. B.; Clavaguera, C.; Ohanessian, G. *J. Phys. Chem. Lett.* **2012**, *3*, 3320.

(46) Morrison, L.; Somogyi, Á.; Wysocki, V. H. *International Journal of Mass Spectrometry* **2012**, *325–327*, 139.

(47) Pan, J.; Heath, B. L.; Jockusch, R. A.; Konermann, L. *Anal. Chem. (Washington, DC, U. S.)* **2012**, *84*, 373.

(48) Gucinski, A. C.; Chamot-Rooke, J.; Nicol, E.; Somogyi, A.; Wysocki, V. H. *J. Phys. Chem. A* **2012**, *116*, 4296.

(49) Paizs, B.; Suhai, S. *Rapid Commun. Mass Spectrom.* **2002**, *16*, 375.